RSC Advances

ROYAL SOCIETY OF CHEMISTRY

www.rsc.org/advances

cite this: DOI: 10.1039/c0xx00000x

www.rsc.org/xxxxxx

ARTICLE TYPE

Evidence for changes on the lithium conduction dimensionality of $Li_{0.5-y}Na_yLa_{0.5}Nb_2O_6$ ($0 \leq y \leq 0.5$) perovskites

Ricardo Jiménez[a*], Virginia Díez[a] and Jesús Sanz[a]
Sofia D. Kobylianska[b], Oleg I. V'yunov[b] and Anatolii G. Belous[b]

Received (in XXX, XXX) Xth XXXXXXXXX 20XX, Accepted Xth XXXXXXXXX 20XX
DOI: 10.1039/b000000x

Abstract

$Li_{0.5-y}Na_yLa_{0.5}\square Nb_2O_6$ samples (y = 0-0.5) were synthesized by the solid-state reaction (SSR). Structural features of the $a_p x a_p x 2a_p$ perovskite series were investigated by X-ray diffraction (XRD), nuclear magnetic resonance (NMR) and density functional theory DFT simulation techniques. The location of La ions was assessed by Rietveld analysis of XRD patterns, and structural sites occupied by Li, Na and Nb ions investigated by MAS-NMR spectroscopy. In Li-rich samples, La and Li ions are preferentially located at z/c = 0 planes, but as Na content increases, La and Na occupy both z/c = 0 and 0.5 planes. To analyze La and Li possible arrangements, different structural models have been considered in DFT simulations, confirming the cation ordering deduced from XRD patterns and the impediment of Na ions to move through square windows of the perovskite. Structural information deduced has been used to discuss transport properties deduced by Impedance Spectroscopy (IS). In Li rich samples, La arrangement in alternating planes favors a 2D-dimensional Li conductivity. The incorporation of Na in two crystallographic planes reduces La ordering and increases Li conductivity. La disorder favours the change from 2D to 3D Li conductivity, that could explain the broad maximum detected in Li conductivity as a function of the Na content.

Introduction

Lithium-conducting materials are of great interest due to their potential use as electrolytes or electrode materials in electrochemical devices such as sensors, rechargeable batteries, miniature supercapacitors and electrochromic displays[1]. One of the most interesting reported lithium-conducting materials is based on $Li_{3x}La_{2/3-x}TiO_3$ perovskites (hereafter named LLTO) that display high conductivity (10^{-3}S.cm^{-1}) and diffusion coefficients ($\approx 10^{-8}$ cm^2/s) at room temperature [2-8]. In literature, it is accepted that the increment of the number of nominal vacancies (n_v) favors ionic conductivity of perovskites. The replacement of Ti by Nb in B positions of perovskites should increase the conductivity in the analogue $Li_{0.5+3x}La_{0.5-x}Nb_2O_6$ series, however, a decrease was observed despite higher amount of vacancies[9].

In LLTO series, Li ions are located at unit cell faces of perovskites, making that the total amount of effective vacancy that participate in conduction, $n_t = [Li] + n_V$, increases[8,10]. In LLTO samples, the substitution of Li by Na decreased slightly conductivity for low Na contents, but drastically when the amount n_t approaches the 3D percolation threshold of conduction networks[10,11]. Previous studies performed on Li conductivity of the $Li_{0.5-y}Na_yLa_{0.5}\square Nb_2O_6$ (LNLNO) series showed that the influence of Na was different, increasing Li conductivity for moderate Na substitutions[9] before decreasing for larger ones. This anomalous behavior pointed to the possibility that the strong detrimental percolative effect, expected for Li substitution by Na, was not occurring in this series[12] and cation vacancies played a different role.

Multinuclear ^{7}Li and ^{23}Na NMR spectroscopy is a useful technique to analyze mobility and structural sites occupied by atoms. In particular, the analysis of quadrupole interactions in MAS-NMR spectra of $Li_{0.5-y}Na_yLa_{0.5}\square TiO_3$ allowed the identification of structural sites occupied by alkaline cations in LLTO perovskites[13]. On the other hand, lithium exchange processes between structural sites afforded information about Li motion mechanisms in perovskites [14, 15]. In $Li_{0.5-y}Na_yLa_{0.5}\square TiO_3$ (LLTO) series, ^{7}Li MAS-NMR spectroscopy was finally used to determine the amount of Li that participate to long-range conductivity near the percolation threshold of vacancies[10].

In this work, the dependence of Li conductivity on structural features of $Li_{0.5-y}Na_y\ La_{0.5}Nb_2O_6$ (y = 0 - 0.5) series has been investigated. Structural characteristics of perovskites will be first analyzed by X-ray and NMR; then Li mobility will be investigated by NMR and Impedance techniques. In these perovskites, niobium and lanthanum location was deduced by Rietveld analysis of XRD patterns. On the other hand, structural sites occupancy by alkaline and niobium atoms was investigated ^{7}Li, ^{23}Na and ^{93}Nb MAS-NMR spectroscopy. DFT simulations were used to estimate possible cation ordering and octhedral tilting schemes, non accessible by XRD. Structural information deduced will be used to analyze the influence of vacancy/La ordering on Li conductivity of $Li_{0.5-y}Na_y\ La_{0.5}\ Nb_2O_6$ series. The conclusions deduced here will be compared with those reported in LLTO series, where a change from 2D to 3D conductivity was detected for increasing Li contents.

Experimental

High-purity La_2O_3, Nb_2O_5, Li_2CO_3, Na_2CO_3 were used as starting reagents. The synthesis procedure is described in detail elsewhere[16, 17]. Samples were first pressed and calcined at 970 K for 4 hours; after grinding, samples were calcined 2h at 1320 K. The samples sintering (2h) was carried out in the temperature range 1470 – 1550 K. The composition of analyzed samples is given in Table I. The density of final ceramics, deduced by the Archimedes method, was between 4.88–5.05 g/cm^3 (relative densities above 95%).

After preparation, ceramics samples were dissolved to perform chemical analyses[17]. Lithium content was deduced by absorption spectroscopy, lanthanum by complexometry, and niobium determined gravimetrically by precipitation with ammonia. According to these analyses some amount of lithium was always lost in preparation of samples.

Table I. Sample composition.

Nominal composition	Experimental composition
$Li_{0.5}La_{0.5}Nb_2O_6$	$Li_{0.400}La_{0.504}Nb_2O_{5.956}$
$Li_{0.4}Na_{0.1}La_{0.5}Nb_2O_6$	$Li_{0.32}Na_{0.067}La_{0.506}Nb_2O_{5.952}$
$Li_{0.3}Na_{0.2}La_{0.5}Nb_2O_6$	$Li_{0.24}Na_{0.18}La_{0.505}Nb_2O_{5.956}$
$Li_{0.2}Na_{0.3}La_{0.5}Nb_2O_6$	$Li_{0.16}Na_{0.28}La_{0.504}Nb_2O_{5.976}$
$Li_{0.1}Na_{0.4}La_{0.5}Nb_2O_6$	$Li_{0.08}Na_{0.375}La_{0.503}Nb_2O_{5.982}$
$Li_{0.07}Na_{0.43}La_{0.5}Nb_2O_6$	$Li_{0.06}Na_{0.414}La_{0.503}Nb_2O_{5.993}$
$Li_{0.04}Na_{0.46}La_{0.5}Nb_2O_6$	$Li_{0.038}Na_{0.449}La_{0.503}Nb_2O_{5.996}$
$Li_{0.02}Na_{0.48}La_{0.5}Nb_2O_6$	$Li_{0.017}Na_{0.46}La_{0.503}Nb_2O_{5.993}$

The crystalline phases were identified by X-ray powder diffraction (XRD) technique. For that, XRD patterns were recorded at room temperature on a DRON-4-07 apparatus (Cu Kα radiation; 40 kV, 18 mA) in the 10-120° 2θ range with a $\Delta 2\theta = 0.02°$ step and an exposure time of 6 s per point. Unit cell parameters were determined by using the Le Bail technique and structural refinements performed with the Rietveld method (Fullprof program) [18].

Taken into account small scattering factors of oxygen atoms, octahedral tilting schemes associated to different arrangements of La/(Li,Na) cations were investigated with DFT techniques (CASTEP software)[19]. The use of Density Functional Theory (DFT) code, which employs the gauge including the projector augmented wave (GIPAW)[20] algorithm, enabled the reconstruction of all-electron wave functions. The Generalized Gradient Approximation (GGA) PBE [21] functional was used and core-valence interactions described by ultrasoft reported pseudo-potentials [22].

Structural parameters (unit cell and atomic positions) deduced by XRD in literature ICSD 180636 (for LaNaNbO) and 99312 (for LaLiNbO) were used for DFT calculations. The crystal structure was reproduced by using periodic boundary conditions. In simulations, different super-lattices, compatible with cation distributions, were considered. For optimization of atomic positions, numerical integrals were performed over the Brillouin zone, using a Monkhorst–Pack grid with a k-point spacing of 0.04 $Å^{-1}$. Wave-functions were expanded in plane waves with a kinetic energy smaller than the cut-off energy, 1200 eV.

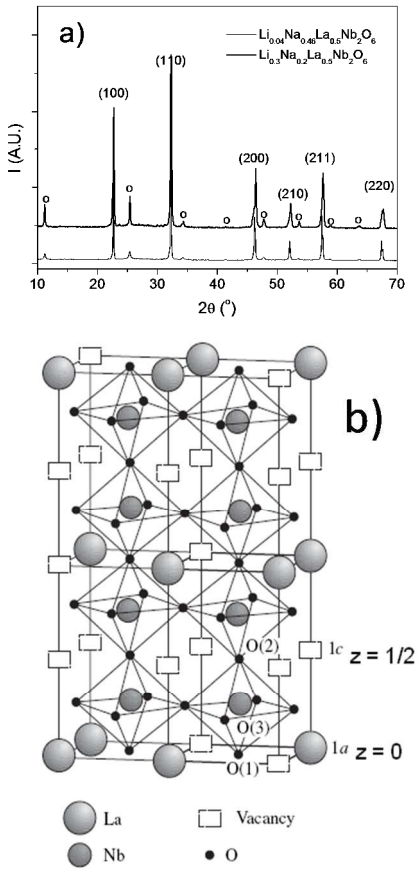

Figure1: a) XRD patterns of two members of the $Li_{0.5-y}Na_yLa_{0.5}\square Nb_2O_6$ series (y=0.2 y=0.46). The (o) symbol indicates super-lattice reflections. b) structure of the deficient perovskite $Li_{0.5}La_{0.5}\square Nb_2O_6$ deduced by Rietveld refinement. In this structure vacancy and La-rich planes alternate along the c-axis.

^{93}Nb, ^{23}Na and ^{7}Li MAS-NMR spectra were recorded at 97.94, 105.8 and 155.51 MHz in a MSL- 400 spectrometer. Samples were rotated at 12 kHz around an axis inclined 54º44' with respect to the external 9.4 T magnetic field (MAS technique). NMR spectra were recorded after 3 µs single pulse irradiation and 10 s recycling. The number of accumulations was 100, 50 and 50 in Nb, Na and Li NMR spectra. NMR components were referred to external $Nb(O)Cl_3$, NaCl and LiCl references. The Winfit program was used for NMR spectra deconvolution. To analyze spinning sideband patterns, more enlarged spectral regions and filters (1 MHz) than used in central components (100 kHz), were considered.

The electrical properties of ceramic samples as a function of temperature were investigated by Impedance Spectroscopy (IS) in the frequency range 20 Hz-1MHz, using an Agilent E4192A analyzer. For low frequency measurements (1mHz–10 kHz) a Zhaner IM6ex apparatus was used. The pellets used in electric determinations were 0.9±0.1 cm in diameter and 0.3±0.02 cm in thickness. Electrical contacts (gold paste) were deposited on the larger surfaces of the pellets and heated at 1125 K. The electronic conductivity measured at 570 K and 0.5 V was 0.05% of the total conductivity. To get more accurate values of the conductivity dispersion, the samples were also measured at room temperature between 1MHz and 3GHz using an E4991A Impedance materials analyzer.

cite this: DOI: 10.1039/c0xx00000x

www.rsc.org/xxxxxx

ARTICLE TYPE

Table II Structure parameters as a function of sodium content (y) in $Li_{0.5-y}Na_yLa_{0.5}\square Nb_2O_6$.

y	0	0.1	0.2	0.3	0.4	0.43	0.46	0.48	0.5
Unit cell parameters									
a, Å	3.9002(1)	3.903(8)	3.906(8)	3.915(1)	3.915(9)	3.923(1)	3.918(1)	3.9167(8)	3.925(1)
b, Å	3.9005(2)	3.904(7)	3.907(8)	3.912(1)	3.915(9)	3.9311(6)	3.923(1)	3.9304(7)	3.9278(6)
c, Å	7.8521(2)	7.854(2)	7.852(1)	7.861(1)	7.861(1)	7.850(2)	7.860(2)	7.846(2)	7.848(3)
V, Å3	119.452(6)	119.7(3)	119.8(4)	120.40(5)	120.5(2)	121.07(5)	120.79(6)	120.78(4)	120.98(6)
Coordinates of ions									
Nb, z/c	0.2580(2)	0.254(2)	0.256(1)	0.256(1)	0.259(1)	0.2527(8)	0.2551(9)	0.2582(9)	0.251(1)
O3, z/c	0.232(1)	0.24(2)	0.30(4)	0.26(2)	0.3(3)	0.28(1)	0.26(4)	0.260(6)	0.29(4)
O4, z/c	0.232(1)	0.21(2)	0.28(4)	0.29(2)	0.3(3)	0.29(1)	0.26(4)	0.272(7)	0.28(4)
Site occupancies (La)									
z = 0	0.487(2)	0.450(9)	0.424(8)	0.362(9)	0.360(9)	0.349(8)	0.349(9)	0.345(7)	0.260(9)
z = 1/2	0.017(2)	0.056(9)	0.081(8)	0.142(9)	0.143(9)	0.154(8)	0.154(9)	0.158(7)	0.243(9)
Agreement factors									
Rf, %	9.14	6.42	6.98	5.92	5.36	7.36	6.30	5.94	6.40
Rexp,%	6.98	8.62	9.15	9.78	8.36	5.01	4.84	4.18	8.96

Results

Crystalline structure

XRD patterns of defective $Li_{0.5-y}Na_yLa_{0.5}\square Nb_2O_6$ ($0 \le y \le 0.5$) perovskites correspond to those of single-phase patterns. For higher Li contents, however, XRD patterns display a small impurity of a Li rich secondary phase (ilmenite). The Fullprof software was used to refine unit cell parameters (Le Bail technique) in orthorhombic (S.G. Pmmm) symmetry. In general unit cell volume increases with increasing y values (Vegard's law), displaying some departure for y values larger than 0.4 (see table II). The structural refinement of $Li_{0.5-y}Na_yLa_{0.5}Nb_2O_6$ perovskites was performed with the Rietveld technique. A doubled $a_p \approx a_p$ x $2a_p$ unit-cell (S.G. Pmmm) was chosen to describe La and vacancies

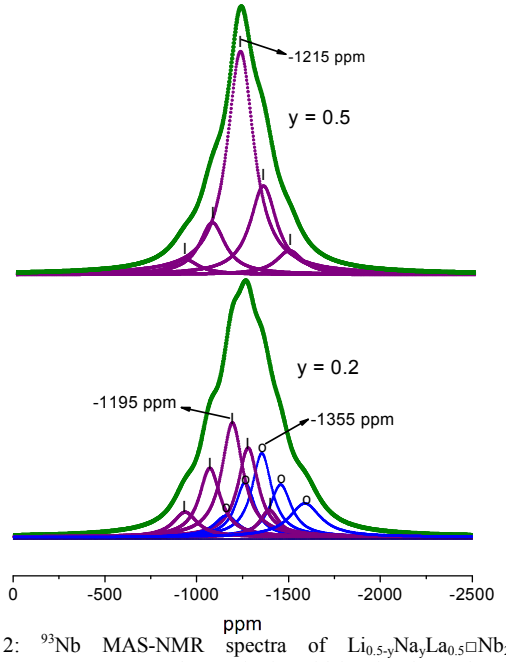

Figure 2: ^{93}Nb MAS-NMR spectra of $Li_{0.5-y}Na_yLa_{0.5}\square Nb_2O_6$ perovskites, y= 0.2, y 0.5, where spinning sidebands of two detected components are indicated.

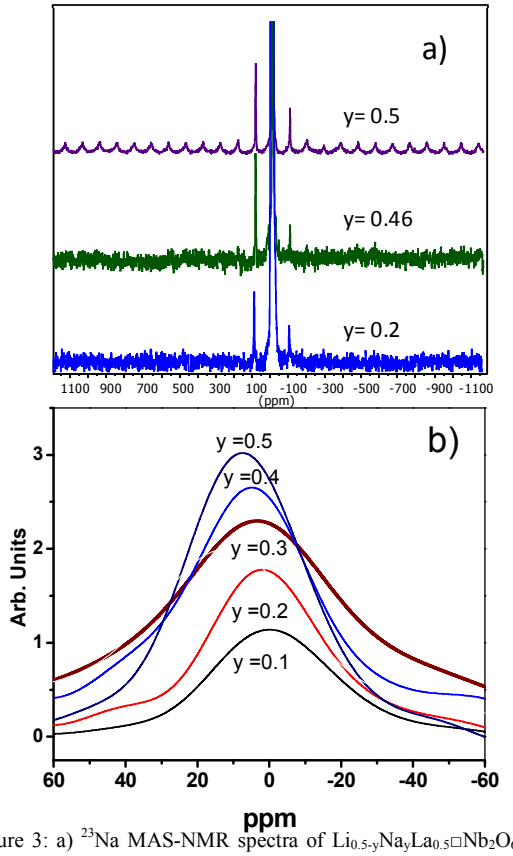

Figure 3: a) ^{23}Na MAS-NMR spectra of $Li_{0.5-y}Na_yLa_{0.5}\square Nb_2O_6$ (y = 0.2, 0.46, 0.5) perovskites. b) central transition of analyzed samples.

ordering along the c axis, previously proposed by Tori et al. for $La_{0.33}NbO_3$ crystals[23]. In this model, a preferential location of

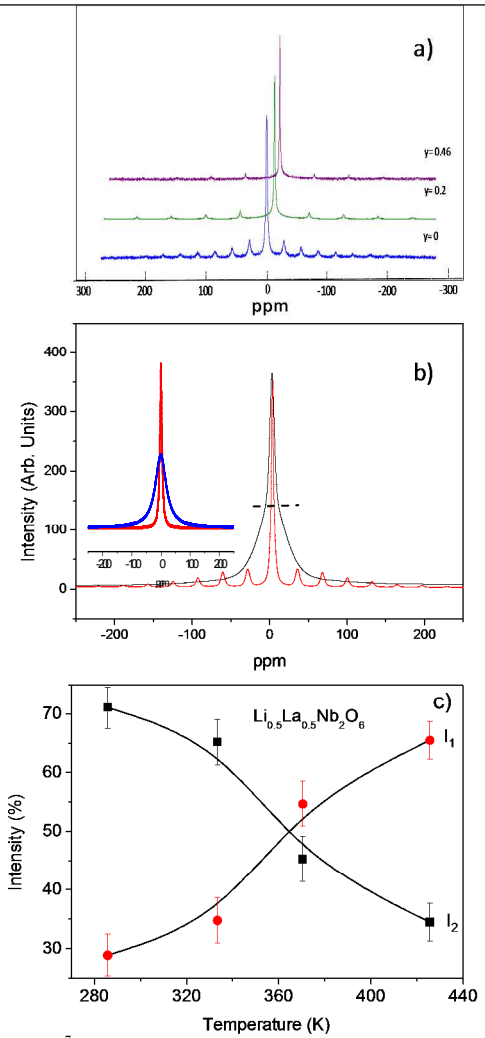

Figure 4:a) ^{7}Li MAS-NMR spectra of $Li_{0.5-y}Na_yLa_{0.5}\square Nb_2O_6$ perovskites, y = 0, 0.2 y 0.46. b) The presence of two components in spectra with and without sample spinning is illustrated, in the inset the deconvolution of two ^{7}Li NMR components is included. c) Relative intensities of Li MAS-NMR narrow (I1) and broad (I2) components as a function of temperature (see text).

vacancies in z/c= 1/2 and La/Li in z/c = 0 planes was proposed. Besides reflections of the doubled unit-cell, some tiny reflections detected in 35-45 ° 2θ region, supports the existence of larger super-lattices deduced by TEM [24]. In this study, octahedral tilting and La/vacancy ordering were invoked to explain the $3.5\sqrt{2}a_p \times \sqrt{2}a_p \times 4a_p$ unit-cell deduced. The intensity of the small reflections (denoted with (o) in Figure 1a) decreased with the Na content, suggesting the progressive La disordering along the series.

Taken into account small intensity of super-lattice reflections, the orthorhombic $a_p \approx a_p \times 2a_p$ unit cell (Pmmm S.G.) was retained to analyze XRD patterns. Atomic coordinates of $Li_{0.5}La_{0.5}\square Nb_2O_6$ perovskite[25] were used as starting model in Rietveld refinements. In this model, La occupy 1a (000), Nb 2t (1/2 1/2 z), O(1) 1f (1/2 1/2 0), O(2) 1h (1/2 1/2 1/2), O(3) 2s (1/2 0 z), O(4) 2r (0 1/2 z) and vacancies 1c (0 0 1/2) sites. In Figure 1b, different occupancy of z=0 and z/c = ½ planes is illustrated.

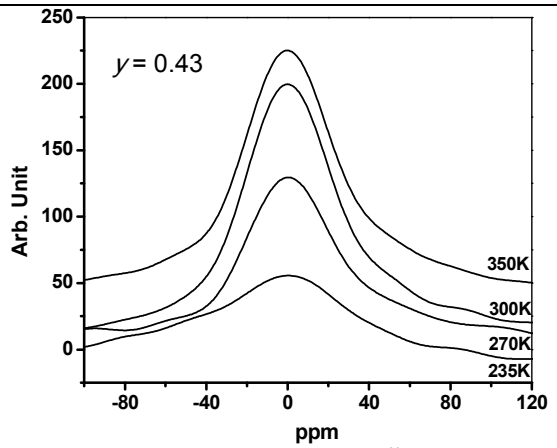

Figure 5: Variation of the central transition of ^{23}Na MAS-NMR spectra of the as a function of temperature in $Li_{0.5-y}Na_yLa_{0.5}\square Nb_2O_6$, y = 0.43, perovskite.

The Rietveld analysis of the $Li_{0.5}La_{0.5}\square Nb_2O_6$ series indicates that La ions occupy preferentially z/c= 0 planes in Li-rich samples, but they are randomly distributed in Na rich samples. As a consequence of the La-vacancy ordering, Nb atoms are shifted from the centre of octahedra. In Na-rich samples, La was disordered in z/c= 0 and ½ planes. In structural analyses, location of Li and Na ions was difficult to deduce, requiring NMR to investigate sites occupation and DFT technique to deduce structural features.

NMR study

^{93}Nb (I=9/2) MAS-NMR spectra should be formed by nine transitions, modulated by spinning sidebands produced by the sample rotation. However, ^{93}Nb MAS-NMR spectra only display the central ½,-½ transition, see Figure 2. The absence of lateral transitions is associated to the presence of structural disorder around Nb octahedra that enlarges considerably quadrupolar transitions. For quantitative analysis of spectra, equally spaced spinning sidebands were considered. The analysis of NMR spectra suggests the existence of one component in Na rich members, but several ones (at least two) in Li rich samples.

^{23}Na (I=3/2) MAS-NMR spectra are formed by three quadrupole transitions, modulated by spinning side bands. In Na-rich samples (y= 0.5), sidebands corresponding to three transitions were detected; however, only the central ½,-½ transition was detected in Li doped samples (Figure 3a). In Na rich members, the central transition was appreciably narrowed, indicating that Na sites at z/c= 0 and ½ planes display similar characteristics (Figure 3b). In y= 0.3 sample, the maximum disorder was produced around Na cations, enlarging considerably central transitions. In this spectrum (y=0.3), the presence of two Na signals, probably associated with two structural planes, was deduced

^{7}Li (I=3/2) MAS-NMR spectra are formed by three transitions, modulated by spinning sidebands of samples rotation (Figure 4). In this figure, it was observed that line width of the central transition and intensity of sidebands decrease as a consequence of Li mobility (Figure 4a). In all cases, intensities of detected bands do not correspond to the quadrupole profile of a single component. In Figure 4b, the presence of two components required to reproduce static and MAS spectra is illustrated. The spectra deconvolution of perovskites was based on the existence of two Li species with different mobility. In Na-doped samples the amount of mobile Li species is considerably higher than in Li-rich members.

In Figure 4c, relative intensities of narrow (line 1) and broad (line 2) components of the sample $Li_{0.5}La_{0.5}\square Nb_2O_6$ are plotted as a function of temperature. The progressive decrease of line-width observed in ^{7}Li MAS-NMR spectra of Na-doped samples must be related to the increment of Li mobility. On the contrary, the ^{23}Na line-width of the central transition of $Li_{0.07}Na_{0.43}La_{0.5}\square Nb_2O_6$ does not change appreciably with temperature, indicating that Na display a lower mobility than Li cations (Figure 5). This difference must be related to Na^+ radius that impedes diffusion of Na ions to pass through square windows that relate contiguous A-sites of the perovskite.

DFT simulations

In this work, we have first analyzed La ordering deduced by XRD in end-members of the series $Li_{0.5-y}Na_yLa_{0.5}Nb_2O_6$. In Li-rich samples, alternating vacant and fully occupied planes favors the Nb shift along c-axis. To take into account ordered models proposed in ab planes[24], $2a_p,a_p,2a_p$ and $2a_p,2a_p,2a_p$ super-lattices with Pmmm symmetry were considered. In the first case, linear arrangements of La and Li produce the octahedral tilting of +/-10º around b-axis; in the second case, the chessboard arrangement of La and Li does not produce a significant tilting. In both cases, two apical Nb-O distances are near 1.91 and 2.05 Å and equatorial ones near 1.97 Å. The analysis of oxygen charges indicates that electron density is redistributed in different oxygens as a consequence of the Nb shift. In both analyzed models, apical oxygens have -0.67 and -0.74 charges and equatorial ones are near -0.72.

In the Na-rich member $Na_{0.5}La_{0.5}\square Nb_2O_6$, ordered lines or chessboard arrangements were again considered. In the case of linear arrangement of La and Na, the tilting was +/- 4º around b-axis; but in the chessboard arrangement no appreciable tilting was detected. In Na phases, octahedra are much less distorted than in Li ones. In both cases, apical Nb-O distances are 1.94 and 2.01 Å while equatorial distances near 1.98 Å. In both models, apical oxygens have -0.67 and -0.71 and equatorial ones near 0.70 charges.

To simulate La/Na disordering, a bigger $2a_p,2a_p,4a_p$ super-cell (P4/mmm S.G.) was considered. The optimized structure showed similar Na coordinations in z/c= 0 and ½ planes and negligible octahedral tiltings. In this model, all Nb-O distances were between 1.97 Å and 2.02 Å. The charge of oxygen atoms were near -0.71 charges. Compared with XRD results the gradual disappearance of the super-cell reflections on increasing the Na substitution is in agreement with the strong La/Na disordering deduced by DFT simulations in the pure Na perovskite. From these simulations, it must be concluded that all ordered models display similar energy values. In order to get more conclusive results on cation / vacancy ordering, structural techniques more sensitive to light atoms should be used.

Ionic conductivity

Ionic conductivity of $Li_{0.5-y}Na_yLa_{0.5}\square Nb_2O_6$ samples has been investigated as a function of the Na fraction, f = [Na]/[Li]+[Na]. The detection of blocking effects at gold-electrodes in all samples, is characteristic of ionic mobile species. In analyzed samples, dc-conductivity presents a larger grain-boundary contribution than the bulk one. The bulk conductivity was extracted from impedance data, by using the "derivative criterion"[26]. In Figure 6a, "bulk" conductivity of different perovskites is plotted as a function of the inverse of the temperature (Arrhenius plots). In general, Li conductivity increases when activation energy (Ea) decreases; however these predictions are not respected in analyzed perovskites, Figure 6b and 6c. When lithium is substituted by sodium in $Li_{0.5-y}Na_yLa_{0.5}Nb_2O_6$ series, ion conductivity measured at 290K increased from $\sigma = 6.85\cdot10^{-6}$ S cm^{-1} (f= 0) to $\sigma = 1.28\cdot10^{-5}$ S cm^{-1} (f = 0.4), decreasing in a non-linear way to 4.10^{-7} S.cm^{-1} when the

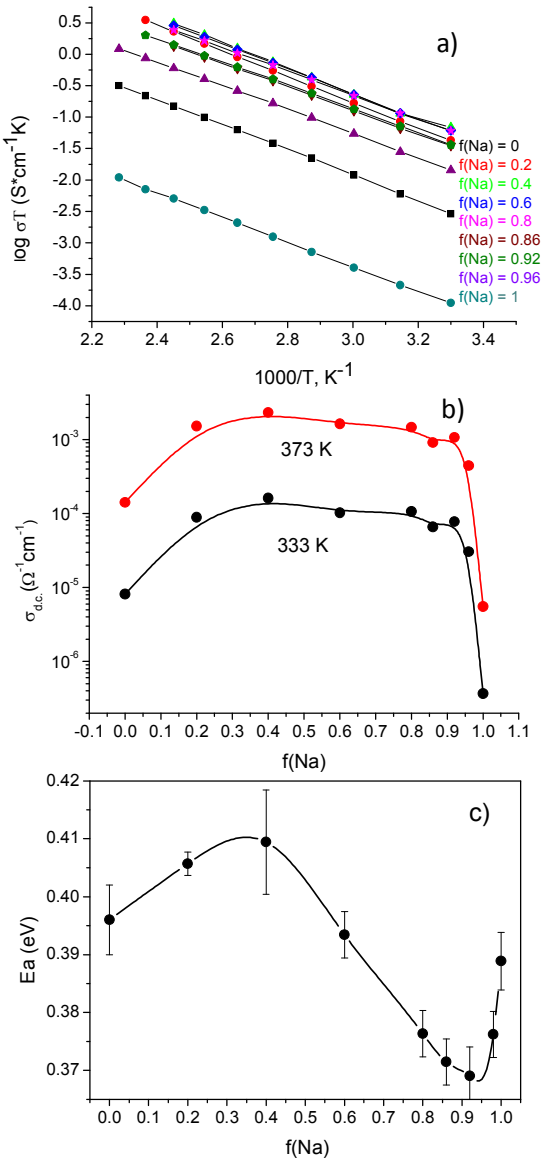

Figure 6: a) Arrhenius plot of conductivity in $Li_{0.5-y}Na_yLa_{0.5}\square Nb_2O_6$, (1) y= 0; (2) y= 0.2; (3) y= 0.3; (4) y= 0.4; (5) y = 0.43; (6) y = 0.46 samples. b) Dependence of dc-conductivity at 333 K (black) and 373 K (red symbols) on the Na fraction of samples. c) Dependence of activation energy on f(Na) values.

Na content increases. In Li-rich samples, activation energy increased from 0.39 to 0.41 eV with the Na fraction ($0 < f < 0.4$), decreasing to 0.37 eV for Na fractions comprised between 0.6 and 0.9, see Figure 6c. In Na-richest samples, activation energy increased again to 0.39 eV. It is interesting to note small variations of conductivity produced in the fraction range $0.2 \leq f[Na] \leq 0.98$, Figure 6b. This is an unexpected result that indicates that the Li conductivity along the series differs from that found in $Li_{0.5-x}La_{0.5}Na_xTiO_3$ series[14,15].

Discussion

Structural features

XRD patterns of $Li_{0.5-y}Na_y\ La_{0.5}\square Nb_2O_6$ perovskites showed the progressive increment of unit cell parameters with the sodium content. The linear variation of unit-cell parameters is usually ascribed to the random distribution of cations in solid solutions (Vegard's law); in our case, however, the variation of the cell volume only follows a linear trend until y=0.4, then the cell volumes departs from expected values. Structural XRD refinements performed here showed that La ions occupy preferentially z/c= 0 planes in Li-rich samples, and randomly distributed in z/c = 0 and ½ planes of Na-rich samples. The changes observed on the La distribution should be related to changes from 2D to 3D Li conductivity and could explain the departure from the Vegard's law.

In ^{93}Nb MAS-NMR spectra, nine quadrupolar transitions should be observed; however, only the central ½,-½ transition was detected. This effect must be ascribed to cation disorder produced around Nb cations, Figure 2. The analysis of ^{93}Nb NMR spectra suggests the existence of one component in Na rich members, but several ones (at least two) in Li rich samples. This information agrees with that deduced from DFT calculations that showed that Nb-O distances differ more in Li- than in Na-rich phases. In Li-rich samples, the location of La in alternate planes produces the shift of Nb ions towards vacant-rich planes; however, in Na-rich samples the simultaneous occupation of z/c= 0 and ½ planes by La and Na cations reduces octahedral distortions and only one ^{93}Nb component was detected. From this fact, differences on the Nb shift along the c-axis (structural disorder) seems to be the reason for additional Nb components.

DFT simulations were oriented to investigate different La/(Li,Na) arrangements in perovskites. In the Li-rich member $Li_{0.5}La_{0.5}\square Nb_2O_6$, the alternation of La and Li arrows in z/c= 0 planes ($2a_p$ x a_p x $2a_p$), produces octahedral tilting is near +/-10º and rhombic distortion of square windows. In chessboard La, Li configurations ($2a_p$ x $2a_p$ x $2a_p$), octahedral tilting should be considerably reduced. Despite DFT results are not conclusive, the existence of La ordering in alternate planes (c= 2 a_p) always produces the shift of Nb atoms, favoring a 2D conductivity. Taken into account the square window size, Li motion is favored with respect to that of Na ions, making that only Li ions must be considered to explain transport properties.

In Na-rich $Li_{0.5}La_{0.5}\square Nb_2O_6$ sample, ^{23}Na MAS-NMR spectra showed the presence of quadrupole transitions, characteristic of well defined interactions of Na ions with the perovskite network oxygens. The detection of a single component indicates that two structural sites occupied by Na ions display similar characteristics. When Na content decreases, quadrupole interactions decrease because Li mobility averages electrical field anisotropies detected by Na ions. The decrease on the residence time on Li sites is responsible for cancellation of quadrupolar ^{7}Li interactions. For intermediate compositions, the spectral broadening detected suggest the partial occupation of z/c= 0 and ½ by Na cations. In Li-rich samples, the narrowing of the shifted Na component suggests that Na ions preferentially occupy the vacancy-rich plane.

Li mobility

When lithium is substituted by sodium in $Li_{0.5-y}Na_yLa_{0.5}Nb_2O_6$ series, ion conductivity increases passing through a broad maximum at (f = 0.4). Besides, activation energy increased from 0.39 to 0.41 eV with the Na fractions (0 < f < 0.4), decreasing to 0.37 eV for Na fractions comprised between 0.6 and 0.9, see Figure 6c.

Li conductivity and activation energy deduced for $Li_{0.5}La_{0.5}Nb_2O_6$ are similar to those reported previously for the same composition (1.10^{-5} S.cm^{-1} and 0.37 eV)[27]. The study of the temperature dependence of NMR relaxation T_1 and T_2 times showed the presence of two Li motions that were assigned to fast motions inside A-cavities and slow motions between contiguous A-cavities[28]. In our work, ^{7}Li NMR spectra show the presence of two types of lithium that display different mobility (Figure 4b).Taken into account structural features of analyzed compounds, the existence of two components could be tentatively assigned to Li motions in vacancy-rich (z/c=1/2) and La-rich (z/c= 0) planes. A 2D-mobility was also invoked by Latie and col. to explain NMR relaxation in $Li_xLn_{1/3}Nb_{1-x}Ti_xO_3$ series[29].

In Li-rich $Li_{0.5}La_{0.5}Nb_2O_6$ sample, the line-width of two ^{7}Li MAS-NMR components is different indicating that Li ions display lower mobility in z/c= 0 (La-rich) planes than in z/c= 0.5 (vacancy rich) planes. The fraction of mobile Li is about 30% of the total one, see Figure 4c. If it is supposed that mobile Li is located at the vacancy rich plane (z/c= ½), the measured Li conductivity should be close to that of $La_{0.6}Li_{0.2}TiO_3$[10]. The low Li conductivity measured in $Li_{0.5}La_{0.5}Nb_2O_6$ ($6.85\ 10^{-6}$ S cm^{-1}) discards this possibility. From this fact, a restricted Li conductivity in La rich planes (z/c = 0 planes) can be assumed.

In the z/c =0 plane, the calculated amount of effective vacancies n_t= Li +vacancy remains below the 2D percolation n_p threshold ($0.5 \leq n_p \leq 0.59$), what should decrease Li conductivity below values detected experimentally. However, measured conductivity values are significant, indicating that the amount of vacancies that participate in Li conduction is higher than considered. Additional vacancies can be produced by La disordering in z/c = 0 and z/c = ½ planes. The partial occupation of z/c= ½ planes was deduced by Rietveld analysis of Li-rich samples, making to increase n_t values above 0.5 in z/c= 0 planes (Table II).

The existence of the two ^{7}Li MAS-MNR components, one mobile and one less mobile has been previously related to Li atoms in z/c = 0 and z/c = ½ planes. The amount of effective vacancy is very close to the percolation threshold for 2D networks in z/c= 0 planes, making that only a fraction of the total Li can participate in the long range mobility. In this situation, most of the Li stay a large residence time in structural sites (broad MNR line component) and only a small amount of Li diffuse along percolated paths. This scenario is supported by the increment of the relative amount of the La fraction in the z/c =1/2 plane and vacancy in z/c = 0 planes, conferring a more isotropic character to Li conductivity on increasing the Na fraction.

Structural information deduced in $Li_{0.5-y}Na_yLa_{0.5}\square Nb_2O_6$ series suggests that Li conductivity changes from 2D (z/c =1/2) to 3D (z/c= 0 and ½ planes) when the Na content increases. However, this change does not affect much "bulk" dc-conductivity that always remains near 10^{-6} S cm^{-1}, Figure 6b. This behavior differs considerably from that reported in Na-LLTO perovskites, where incorporation of Na decrease drastically Li conductivity near the percolation threshold [14,15]. In the series analyzed here, no percolation-controlled phenomena were detected because the important amount of vacant A-sites.

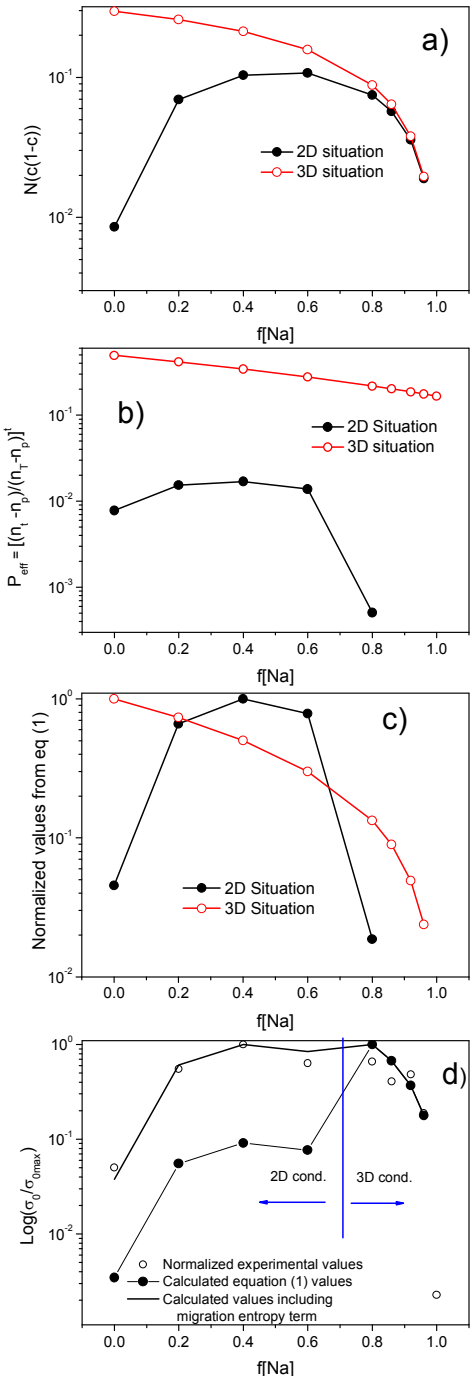

Figure 7: Calculations of pre-exponential values for 2D and 3D regimes. Red lines and symbols stand for 3D and black lines and symbols stand for 2D regimes. Dependences of: a) the N.c.(1-c) factor. b) the percolation efficiency $[(n_t-n_p)/(n_T-n_p)]^t$. c) the normalized conductivity values deduced from expression (1).d) normalized pre-exponential factors. Hollow symbols stand for experimental data, and black circles for values calculated with equation (1) and normalized factors. Upper continuous line stands for calculated values including the corresponding increment in migration entropy produced along the 2D to 3D regime change.

In the analyzed series, the change of La ordering, induced by the increasing Na content, must be related to small effect observed in conductivity. To understand the effect of the Na incorporation on

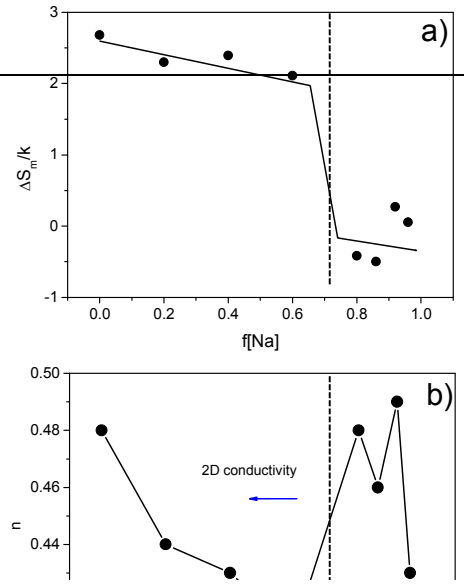

Figure 8: a) Change in the excess of migration entropy in the ordered state ($\Delta S_m/k$) as a function of the Na fraction. b) Variation of the n exponent with the sodium fraction f(Na). The vertical dashed line indicates the change from 2D to 3D ionic conductivity induced by La disorder.

the "bulk" dc-conductivity, the analysis of pre-exponential factors has been performed.

In general, pre-exponential σ_0 factors are proportional to[30]:

$$\sigma_0 \alpha\ N.c(1\text{-}c).[(n_t - n_p)/(n_T - n_p)]^t \qquad (1)$$

where N stands for equivalent Li sites, and c and (1-c) are relative concentrations of Li and vacant sites in structural sites. In this expression, n_t is the effective vacancy concentration, n_p the percolation threshold, n_T the maximum possible number of available sites for the ion movement and t the critical exponent.

In expression (1), N.c(1-c) values provide information about the probability of the lithium hopping between neighboring sites, and $P_{eff} = [(n_t - n_p)/(n_T - n_p)]^t$ takes into account the percolation efficiency in diffusion paths ($0 \leq P_{eff} \leq 1$). The exponent, t, and the percolation threshold, n_p, changes with conduction dimensionality, going from $n_p \geq 0.50$ and $t \approx 1.33$ (two-dimensional) to $n_p \geq 0.31$ and $t \approx 2$ for three-dimensional networks[10]. For Li mobility restricted to z=0 planes the maximum number of sites is 1 but when mobility is extended to both planes, n_T increases to 2.

From Rietveld analysis, different structural parameters can be estimated as a function of the Na fraction. In Figure 7a the evolution of N.c(1-c) vs. Na fraction is considered in 2D (z/c = 0 planes) and 3D (z/c=0 and z/c = ½ planes involved) regimes. The main difference was detected for low f(Na) values: in 2D regime, the N.c(1-c) factor increasing as a consequence of the increment of vacancy in z/c= 0 planes, induced by Na occupation of z/c = ½ planes. In this case, the amount of efficient vacancies is given by $n_t = 1/3+\Delta La+[Li]/3$, where ΔLa stands for La occupation of z/c = ½ planes. In $Li_{0.5}La_{0.5}Nb_2O_6$ composition, a minimum La disorder is required (ΔLa = 0.013) to explain measured Li conductivity. For higher Na fractions, N.c(1-c) decreases as a consequence of the lower occupancy of z/c= 0 planes by lithium. In the 3D regime, the random distribution of La, Li, and Na ions and vacancies is produced, improving considerably N.c(1-c) values. In the random case, $n_t = 1.3+[Li]/3-2[Na]/3$. On increasing the Na content, the N.c(1-c) factor decreases. It is interesting to note that for highest Na concentrations, expected N.c(1-c) for 2D and 3D regimes merge to common values.

The evolution of the percolation efficiency P_{eff} with Na fraction values is analyzed in Figure 7b. In 2D regime, P_{eff} increases up to f = 0.6, (Na ion incorporated at the z= ½ plane) decreasing considerably above this value. For f 0.8, the system becomes sub-percolated ($n_t < n_p$) , and 2D conductivity is not possible, (P_{eff} = 0). In 3D regime, the percolation efficiency is about two orders of magnitude larger than in 2D regime, because the amount of vacancy always remain well above the percolation threshold, making that Na content not to affect strongly conductivity values.

Results deduced from the equation 1, once normalized to maximum 2D and 3D values, are plotted in Figure 7c. In this plot it can be inferred that 2D predictions reproduces well experimental results below f= 0.6, and 3D predictions, those above 0.7. Based on this fact, it is possible to calculate the equation (1), taking into account the proposed change of dimensionality as produced at f[Na]~ 0.7. In Figure7d, calculated and experimental values display similar values for high Na content but calculated ones are below experimental results for 2D regime. As observed in Figure 7b, P_{eff} is very different in 2D and 3D regimes. The Li changes from a restricted mobility along z/c = 0 planes in ordered samples to an easy 3D mobility in disordered samples. The change produced across 2D to the 3D transition must have an important effect on the migration entropy. In order to reproduce properly experimental results, the equation (1) had to consider the migration entropy associated with the effective attempt frequency (ω_e). Using the Almond and West formalism[30] ω_e can be expressed as:

$$\omega_e = \omega_0 \exp(\Delta S_m/k) \qquad (2)$$

making that expression (1) adopt the form:

$$\sigma_0 = N.c(1\text{-}c).[(n_t - n_p)/(n_T - n_p)]^t.\omega_e \qquad (3)$$

where ω_0 is the attempt frequency and $\Delta S_m/k$ is the increment of entropy produced by Li migration. $\Delta S_m/k$ is important in ordered 2D systems, but considerably reduced in disordered 3D regimes. If we calculate the migration entropy factor excess ($\Delta S_m/k$) needed to fit experimental and calculated conductivities, results plotted against the f[Na] showed the shape of an order-disorder transition (Figure 8a). The decrement observed takes into account the migration entropy excess produced from transition between ordered and disordered regimes. The zero value is relative and means that there is no excess in migration entropy over the value of the disordered 3D regime. The maximum value corresponds to the restricted conductivity of the $Li_{0.5}La_{0.5}Nb_2O_6$ sample.

The scenario proposed to explain conductivity is also responsible for the evolution of activation energy depicted in Figure 6c, where Ea increases up to f = 0.6 and then decreases to a minimum for f= 0.9. The increment detected above f = 0.9, was ascribed to low Li contents that impede long-term Li conductivity.

Additional evidences for the suggested change in dimensionality can be found in the analysis of the frequency dispersion of the conductivity. It has been proposed that a dimensionality change affects dispersion exponent n values of the "bulk" a.c. conductivity (σ_{ac}):

$$\sigma_{ac} = \sigma_{dc}[1+ (\omega/\omega_p)^n] \qquad (4)$$

where ω_p stands for the crossover frequency between dc (σ_{dc}) and dispersive regimes. As demonstrated by Sidebottom[32], 2D displays lower n values than 3D regimes. An accurate determination of n is however, a difficult task that requires high frequency IS measurements (1MHz-3GHz). The results deduced from the fitting of experimental values to equivalent circuit reported in reference[31] are included in Figure 8b. Deduced n values decreased from 0.44 to 0.41 when passing from f =0.4 to 0.6. The increment of n to 0.48 in f=0.8 samples, cannot be related to Li correlation effects in z/c=0 planes. Then, a

dimensionality change must be invoked to explain observed values. For Na-rich samples, n values are higher than those corresponding to 2D regimes, despite of low lithium contents.

The analysis of conductivity allows us to suggest that Li conductivity in $Li_{0.5-y}Na_yLa_{0.5}Nb_2O_6$ is affected by two competing factors. For Li-rich samples, incorporation of sodium increases cation disorder and favors the simultaneous Li and La occupation of z/c= 0 and ½ planes, with the resulting 2D to 3D regime change. This change makes the activation energy to decrease and pre-exponential factor to increase, not affecting considerably Li conductivity. In Na-rich samples with f values higher than 0.9, activation energy increase and conductivity decrease as a consequence of low Li contents. Finally, f=1 sample showed ionic conductivity that should be related to the presence of a small amount of mobile Na ions.

Conclusions

$Li_{0.5-y}Na_yLa_{0.5}\square Nb_2O_6$ samples (y = 0-0.5) were synthesized by solid-state reaction (SSR) and transport properties deduced by Impedance spectroscopy. Structural features of samples were deduced by x-ray diffraction (XRD), nuclear magnetic resonance (NMR) techniques and DFT simulations.

La occupation of z/c= 0 and ½ planes was deduced from XRD Rietveld refinements, and distribution of Li, Na and Nb ions assessed by MAS-NMR spectroscopy. In Li rich samples, La and Li ions, are preferentially disposed in alternate planes along the c-axis (2D conductivity). As the Na content increases, La and Na cations occupy z/c = 0 and 1/2 planes and vacancies becomes disordered that can increase the conductivity dimensionality (3D conductivity).

In Li rich samples, the vacancy disorder increases, increasing activation energy and Li conductivity (2D regime) when Na content increases. In Na-rich samples the increased disorder can lead to a ~~(~~3D regime~~)~~, activation energy increasing and total conductivity decreasing. The cation disorder produced along the proposed 2D to 3D transformation would explain the broad conductivity maximum detected at intermediate compositions. To explain observed results, large changes in the migration entropy must be produced along the transformation, that should be related to the change from and ordered to a disordered cation distribution.

Acknowlegdements

This work has been funded by the Spanish projects MINECO MAT2013-46452-C4-2R and MATERYENER3-CM (S2013/ MIT-2753) and the European project NANOLICOM (FP7-PEOPLE-2009-IRSES).

Adresses

[a] *Instituto de Ciencia de Materiales, ICMM-CSIC. C / Sor Juana Inés de la Cruz 3 , 28049, cantoblanco 3 Madrid; *E-mail:riqjim@icmm.csic.es*
[b] *Vernadsky Institute of General and Inorganic Chemistry, National Academy of Sciences of Ukraine, Palladine Ave32-34, 03680Kyiv 142, Ukraine*

References

1 Robertson, A.D.; West, A.R.; Ritchie, A.G. "Review of crystalline lithium-ion conductors suitable for high temperature battery applications".Solid State Ionics. 104 (1997) 1-11.

2 Belous, A.G.; Butko, V.I.; Novitskaya, G.N.; et al "Conductivity of $La_{2/3-x}M_{3x}TiO_3$ perovskites''. Ukrainskii Fizicheskii Zhurnal. 31 (1986) 576-580.

3 Belous, A.G.; Novitskaya, G.N.; Polyanetskaya, S.V.; et al." Study of complex oxides with the composition $La_{2/3-x}Li_{3x}TiO_3$". Inorganic Materials. 23 (1987) 412-415.

4 Inaguma, Y.; Chen, L.Q.; Itoh, M.; et al. "High Ionic-Conductivity In Lithium Lanthanum Titanate".Solid State Communications. 86 (1993) 689-693.

5 Bohnke, O; Bohnke, C; Fourquet, JL "Mechanism of ionic conduction and electrochemical intercalation of lithium into the perovskite lanthanum lithium titanate". Solid State Ionics. 91 (1996) 21-31.

6 Alonso, JA; Sanz, J; Santamaria, J; et al. "On the location of Li^+ cations in the fast Li-cation conductor $La_{0.5}Li_{0.5}TiO_3$ perovskite". Angewandte Chemie-International Edition. 39 (2000) 619-621.

7 Sanjuan, M.L.; Laguna, M.A.; Belous, A.G.; et al. "On the local structure and lithium dynamics of $La_{0.5}(Li,Na)_{0.5}TiO_3$ ionic conductors. A Raman study". Chemistry of Materials. 17 (2005) 5862-5866.

8 Ibarra, J; Varez, A; Leon, C; et al. "Influence of composition on the structure and conductivity of the fast ionic conductors $La_{2/3-x}Li_{3x}TiO_3$ $(0.03 \leq x \leq 0.167)$",Solid State Ionics 134 (2000) 219-228.

9 Belous A., Pashkova E., Gavrilenko O., V'yunov O. and Kovalenko L. "Solid electrolytes based on lithium-containing lanthanum metaniobates", J. Eur. Ceram. Soc. 24 (2004) 1301-1304.

10 Herrero, CP; Varez, A; Rivera, A; et al. "Influence of vacancy ordering on the percolative behavior of $(Li_{1-x}Na_x)_{3y}La_{2/3-y}TiO_3$ perovskites". J. Physical Chemistry B. 109 (2005) 3262-3268.

11 Rivera, A; Leon, C; Santamaria, J; et al. "Percolation-limited ionic diffusion in $Li_{0.5-x}Na_x$ $La_{0.5}TiO_3$ perovskites (0 <= x <= 0.5)". Chemistry of Materials 14 (2002) 5148-5152.

12 Gavrilenko, O. N.; Belous, A. G.; Kovalenko, L. L.; et al. "Effect of the a-site substitution on the structure peculiarities and ionic conductivity of solid electrolytes $La_{2/3-x-y}Li_{3x-y}Sr_{2y}\square_{4/3-2x}$ Nb_2O_6", Materials and Manufacturing Processes 23 (2008) 607-610.

13 Paris, MA; Sanz, J; Leon, C; et al. "Li mobility in the orthorhombic $Li_{0.18}La_{0.61}TiO_3$ perovskite studied by NMR and impedance spectroscopies".Chemistry of Materials. 12 (2000) 1694-1701.

14 Jimenez, R.; Rivera, A.; Varez, A.; et al. "Li mobility in $Li_{0.5-x}Na_xLa_{0.5}TiO_3$ perovskites $(0 \leq x \leq 0.5)$ Influence of structural and compositional parameters".Solid State Ionics, 180 (2009)1362-1371.

15 Jimenez, R.; Varez, A.; Sanz, J. "Influence of octahedral tilting and composition on electrical properties of the $Li_{0.2-x}Na_xLa_{0.6}TiO_3$ (0 <= x <= 0.2) series". Solid State Ionics. 179 (2008) 495-502.

16 A. Belous, O. Gavrilenko, O. Pashkova, O. Bohnké, C. Bohnké. "Structural Peculiarities and Electrophysical Properties of Lithium Ion Conducting Lanthanum Niobate Prepared by Solid-State Reaction and Precipitation from Solution", Eur. J. Inorg. Chem. (2008), 4792-4796

17 Belous, A.G.; Gavrilenko, O.N.; Pashkova, E.V. "Effect of synthesis conditions on the lithium nonstoichiometry and properties of $La_{2/3-x}Li_{3x}\square_{(4/3)-2x}M_2O_6$ (M = Nb, Ta) perovskite-like solids", Inorganic Materials. 40 (2004) 867-873.

18 Rodríguez-Carvajal, J.; Roisnel, T. (1999); FullProf, WinPLOTR and accompanying programs at http:// www-llb.cea.fr/fullweb/powder.htmf

19 Clark, S. J.; Segall, M. D.; Pickard, C. J.; Hasnip, P. J.; Probert, M. J.; Refson, K.; Payne, M. C. Zeitschrift Fur Kristallographie 2005, 220, 567.

20 Pickard, C. J.; Mauri, F. Physical Review B 2001, 63.

21 Perdew, J. P.; Burke, K.; Ernzerhof, M. Physical Review Letters 1996, 77, 3865.

22 Yates, J. R.; Pickard, C. J.; Mauri, F., "Calculation of NMR chemical shifts for extended systems using ultrasoft pseudopotentials". Physical Review B 2007, 76, (2), 024401.

23 Tori, Y.; Seckiya, T.; Yamamoto, T. Mater. Research Bulletin, 17,727, (1983).

24 S. Garcia-Martin; M.A. Alario-Franco. "Modulated Structure of $La_{1/3-x}Li_{3x}NbO_3$ ($0 \leq x \leq 0.06$) Perovskite – Related Materials" J. Solid State Chem. 148, 93-99 (1999).

25 25 Nalbandyan V. B. "Novel oxide in the system La_2O_3-Me_2O_5"/ V. B. Nalbandyan and I. A. Shukaev // Zhurn. Neorg. Khim. 34 (1989) 79-795

26 Bucheli, W.; Jimenez, R.; Sanz, J.; et al. "The log(sigma) vs. log(omega) derivative plot used to analyze the ac conductivity. Application to fast Li^+ ion conductors with perovskite structure", Solid State Ionics. 227 (2012) 113-118.

27 S. Garcia-Martin, J.M. Rojo, H. Tsukamoto, E. Moran and M.A. Alario-Franco, "Lithium-ion conductivity in the novel solid solution with Perovskitas-related structure", Solid State Ionics, 116 (1999) 11-18.

28 Emery, J.; Bohnke, O.; Florian, P. and Marzouk, K. "NMR study of Li^+ ion dynamics in the Perovskitas $Li_{3x}La_{1/3-x}NbO_3$", J. Phys. Chem., 109 (2005) 20680-20689.

29 Latie, L.; Villeneuve, G.; Conte, D. and Le Flem " Ionic conductivity of oxides with general formula $Li_xLn_{1/3}Nb_{1-x}Ti_xO_3$ (Ln= La, Nd)", J Solid State Chemistry, 51 (1984) 293-299.

30 Almond, D.P.; West, AR "The activation entropy for transport in ionic conductors". Solid State Ionics. 23 (1987) 27-35.

31 Bucheli, W.; Duran, T.; Jimenez, R. et al. "On the influence of the vacancy distribution on the structure and ionic conductivity of A-site-deficient $Li_xSr_xLa_{2/3-x}TiO_3$ perovskites", Inorganic Chemistry. 51 (2012) 5831-5838.

32 Sidebottom, DL. "Dimensionality dependence off the conductivity dispersion in ionic materials". Physical Review Letters, 83 (1999) 983-986.